DOI: 10.1002/chem.200700019

Ligand versus Metal Protonation of an Iron Hydrogenase Active Site Mimic

Gerriet Eilers,[a] Lennart Schwartz,[a] Matthias Stein,[b] Giuseppe Zampella,[c] Luca de Gioia,[c] Sascha Ott,*[a] and Reiner Lomoth*[a]

Abstract: The protonation behavior of the iron hydrogenase active-site mimic $[Fe_2(\mu\text{-adt})(CO)_4(PMe_3)_2]$ (**1**; adt = *N*-benzyl-azadithiolate) has been investigated by spectroscopic, electrochemical, and computational methods. The combination of an adt bridge and electron-donating phosphine ligands allows protonation of either the adt nitrogen to give $[Fe_2(\mu\text{-Hadt})(CO)_4(PMe_3)_2]^+$ (**[1H]$^+$**), the Fe–Fe bond to give $[Fe_2(\mu\text{-adt})(\mu\text{-H})(CO)_4(PMe_3)_2]^+$ (**[1Hy]$^+$**), or both sites simultaneously to give $[Fe_2(\mu\text{-Hadt})(\mu\text{-H})(CO)_4(PMe_3)_2]^{2+}$ (**[1HHy]$^{2+}$**). Complex **1** and its protonation products have been characterized in acetonitrile solution by IR, ^{1}H, and ^{31}P NMR spectroscopy. The solution structures of all protonation states feature a basal/basal orientation of the phosphine ligands, which contrasts with the basal/apical structure of **1** in the solid state. Density functional calculations have been performed on all protonation states and a comparison between calculated and experimental spectra confirms the structural assignments. The ligand protonated complex **[1H]$^+$** ($pK_a = 12$) is the initial, metastable protonation product while the hydride **[1Hy]$^+$** ($pK_a = 15$) is the thermodynamically stable singly protonated form. Tautomerization of cation **[1H]$^+$** to **[1Hy]$^+$** does not occur spontaneously. However, it can be catalyzed by HCl ($k = 2.2\ M^{-1}s^{-1}$), which results in the selective formation of cation **[1Hy]$^+$**. The protonations of the two basic sites have strong mutual effects on their basicities such that the hydride ($pK_a = 8$) and the ammonium proton ($pK_a = 5$) of the doubly protonated cationic complex **[1HHy]$^{2+}$** are considerably more acidic than in the singly protonated analogues. The formation of dication **[1HHy]$^{2+}$** from cation **[1H]$^+$** is exceptionally slow with perchloric or trifluoromethanesulfonic acid ($k = 0.15\ M^{-1}s^{-1}$), while the dication is formed substantially faster ($k > 10^2\ M^{-1}s^{-1}$) with hydrobromic acid. Electrochemically, **1** undergoes irreversible reduction at −2.2 V versus ferrocene, and this potential shifts to −1.6, −1.1, and −1.0 V for the cationic complexes **[1H]$^+$**, **[1Hy]$^+$**, and **[1HHy]$^{2+}$**, respectively, upon protonation. The doubly protonated form **[1HHy]$^{2+}$** is reduced at less negative potential than all previously reported hydrogenase models, although catalytic proton reduction at this potential is characterized by slow turnover.

Keywords: density functional calculations · electrochemistry · enzyme models · hydride ligands · tautomerism

Introduction

The conversion of protons into molecular hydrogen and vice versa might be of major importance for future energy technology,[1] and inexpensive catalytic materials for these reactions could be derived from synthetic mimics of hydrogenase enzymes.[2–8,9]

Crystallographic, spectroscopic, and theoretical investigations have revealed a detailed picture of the active sites of these natural catalysts (a in Scheme 1).[10–13] The ligand set of the unusual low-valent diiron subsite in the iron hydrogenases contains carbon monoxide and cyanide ligands and a bridging bis-sulfide provided by an S-CH_2-X-CH_2-S ligand, which is most likely azadithiolate (X = NH) according to computational results.[12] As regards the function of these structural elements, it is apparent that the electron-donating

[a] G. Eilers, L. Schwartz, Dr. S. Ott, Dr. R. Lomoth
Department of Photochemistry and Molecular Science
The Ångström Laboratories, Uppsala University
Box 523, 75120 Uppsala (Sweden)
Fax: (+46) 18-471-6844
E-mail: Sascha.Ott@fotomol.uu.se
Reiner.Lomoth@fotomol.uu.se

[b] Dr. M. Stein
EML Research gGmbH, Molecular and Cellular Modeling
Schloss-Wolfsbrunnenweg 33, 69118 Heidelberg (Germany)

[c] Dr. G. Zampella, Prof. L. de Gioia
Department of Biotechnology and Biosciences
University of Milano-Bicocca
Piazza della Scienza 2, 20126 Milano (Italy)

Supporting Information for this article is available on the WWW under http://www.chemeurj.org/ or from the author.

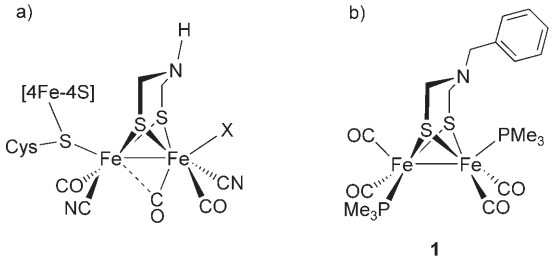

Scheme 1. Structure of the iron hydrogenase active site (a) and the solid-state structure of ($[Fe_2(\mu\text{-adt})(CO)_4(PMe_3)_2]$) (**1**) (b).

cyanides facilitate the formation of a hydride complex by oxidative addition of a proton at the iron center. The central nitrogen atom in the azadithiolate, on the other hand, has been suggested to serve as the basic site that stores the proton that is eventually combined with the hydride to form dihydrogen.[14,15]

Functional studies of synthetic models of the active site have thus far been restricted to complexes containing either of these structural elements, that is, either electron-donating ligands with an all-carbon propyldithiolate (pdt = S-CH_2-CH_2-CH_2-S) bridge or all-carbonyl structures with a nitrogen-containing adt bridge. For the cyano- and/or phosphine-substituted pdt complexes,[16–18] reduction of the μ-hydrido complex results in electrocatalytic hydrogen production at less negative potentials than for their hexacarbonyl analogues,[18–20] where reduction has to precede the oxidative protonation. For the adt all-carbonyl motif,[21] on the other hand, protonation of the bridge nitrogen results in a major shift of the potential required for reduction of the complex that allows for hydrogen formation at potentials even less negative than for the cyanide/phosphine-substituted pdt complexes. It can therefore be anticipated that a complex capable of binding a proton and a hydride in its initial oxidation state would be most easily reduced and potential catalytic turnover should occur at the least negative potential.

We have recently reported the diiron complex $[Fe_2(\mu\text{-adt})(CO)_4(PMe_3)_2]$, which combines the above two structural features in the form of trimethylphosphine ligands and an *N*-benzylazadithiolate (adt) bridge (b in Scheme 1).[22] This combination allows the synthesis of a diiron dithiolate complex $\mathbf{[1HHy]^{2+}}$ that simultaneously carries a hydride on the iron centers and a proton on the nitrogen bridge. Remarkably, two singly protonated forms of the same complex, namely the adt-protonated complex $\mathbf{[1H]^+}$ and hydride $\mathbf{[1Hy]^+}$, can be prepared selectively.

Herein we report full details of the protonation reactions and of the structural characterization of the four protonation states and compare their electrochemical properties.

Results and Discussion

Solution structures: The solid-state structure of **1** was determined by X-ray crystallography[22] and is characterized by a basal/apical conformation of the phosphine ligands, as shown in Scheme 1. To establish the dominant solution structure of **1** we recorded the ^1H and ^{31}P NMR spectra in [D_3]acetonitrile solution. The ^1H NMR spectrum of **1** features a doublet for the trimethylphosphine protons at $\delta =$ 1.50 ppm due to coupling with the phosphorus nucleus.[23] A second doublet of significantly smaller amplitude (ca. 10%) is observed at $\delta = 1.43$ ppm (Figure 1), which seems to suggest that two geometrical isomers are present in solution after dissolving crystalline **1**. Density functional calculations reproduced the solid-state structure of **1**, with good agreement between calculated and experimental interatomic distances and bond angles (data not shown), but also predict that an isomer with both phosphines in a basal position *trans* to each other is almost isoenergetic with the basal/apical isomer found in the solid state. One singlet for the dominant isomer is visible at $\delta = 23.2$ ppm in the proton-decoupled ^{31}P NMR spectrum (Table 1). The presence of only

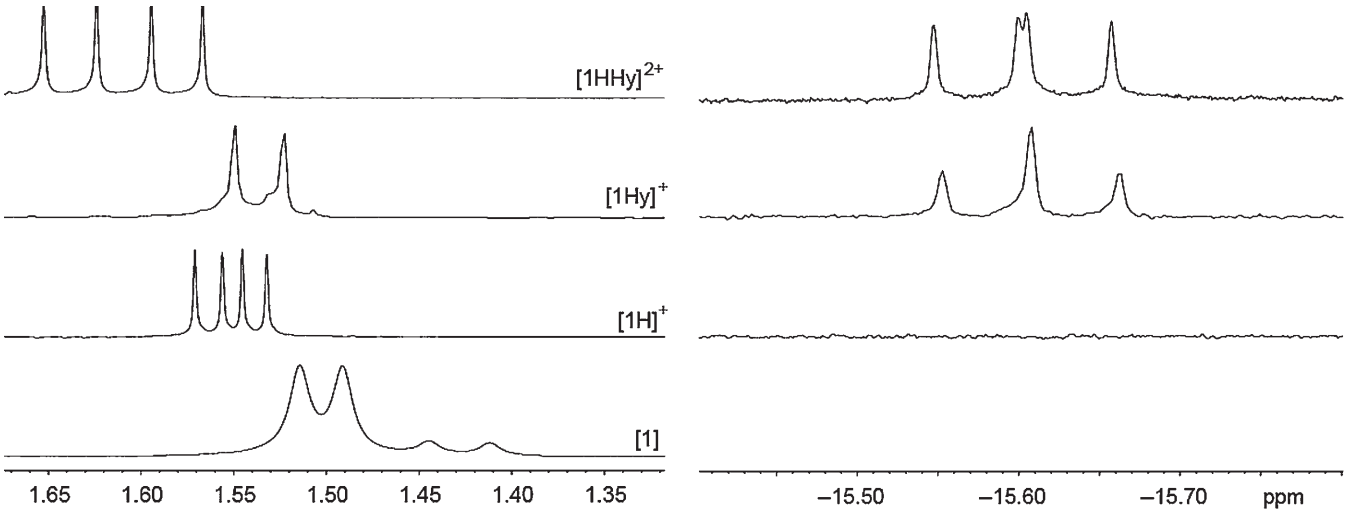

Figure 1. ^1H NMR spectra of **1**, $\mathbf{[1H]^+}$, $\mathbf{[1Hy]^+}$, and $\mathbf{[1HHy]^{2+}}$ prepared from **1** and perchloric, hydrochloric, and triflic acid, respectively in [D_3]acetonitrile at 25 °C. Left: trimethylphosphine region. Right: Bridging hydride region.

one signal of large amplitude points towards a symmetric arrangement around the iron nuclei, which is in contrast to the crystal structure, where the two phosphine ligands occupy dissimilar apical and basal positions. This behavior is consistent with that of the ethyldithiolate-bridged analog of **1**, which also prefers an apical/basal orientation in the solid state and a basal/basal conformation in solution at room temperature.[24,25] The theoretical results provide further support for our assignment as the NMR chemical shifts calculated for the basal/basal isomer match the experimental data. The calculated solution structure of **1** is shown in Scheme 2 together with those of the protonated states. The

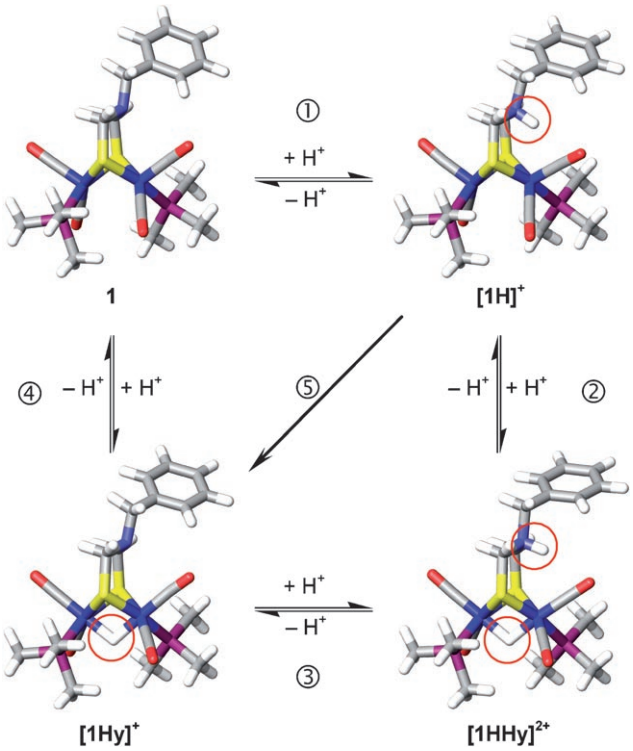

Scheme 2. The protonation states of **1** and their conversion reactions in acetonitrile solution. The geometries are optimized at the B-P86/TZVP level by density functional calculations. Red circles indicate the positions of the proton on the N atom of the adt ligand (**[1H]$^+$** and **[1HHy]$^{2+}$**) and of the hydride ligand bridging the Fe centers (**[1Hy]$^+$** and **[1HHy]$^{2+}$**).

protonated complexes $[Fe_2(\mu\text{-Hadt})(CO)_4(PMe_3)_2]^+$ (**[1H]$^+$**), $[Fe_2(\mu\text{-adt})(\mu\text{-H})(CO)_4(PMe_3)_2]^+$ (**[1Hy]$^+$**), and $[Fe_2(\mu\text{-Hadt})(\mu\text{-H})(CO)_4(PMe_3)_2]^{2+}$ (**[1HHy]$^{2+}$**) can be prepared selectively by the previously reported methods[22] (see also protonation reactions section) and are readily distinguished by their NMR spectra.[22] Protonation of the bridge nitrogen in cation **[1H]$^+$** prevents the inversion of the six-membered azametallaheterocycle and renders the system asymmetric. The two trimethylphosphines at the iron nuclei become nonequivalent and the protons of the respective ligands give rise to two doublets of equal intensity at $\delta = 1.56$ and 1.54 ppm (see Figure 1 and Table 1). Interestingly, the minor isomer that was detected for the non-protonated form is not observable after protonation. Two signals can be detected at $\delta = 31.1$ and $\delta = 19.8$ ppm in the proton-decoupled ^{31}P NMR, thereby reflecting the asymmetry caused by the protonated adt ligand. The former signal is a sharp doublet ($J = 4.7$ Hz) due to coupling to the second, dissimilar phosphine, the signal of which is broader.

The most prominent feature in the ^{1}H NMR spectrum of cation **[1Hy]$^+$** is the resonance of the hydride, which appears at $\delta = -15.6$ ppm as a triplet ($J_{H,P} = 22$ Hz). It can thus be concluded that the hydride resides in a bridging position and that it couples to two equivalent phosphorus centers. Moreover, only one doublet is visible for the trimethylphosphine protons ($\delta = 1.53$ ppm). In the proton-decoupled ^{31}P NMR spectrum (the hydride region is excluded in the decoupling), one doublet ($J_{P,H} = 22$ Hz) is detected at $\delta =$ 21.9 ppm, which further corroborates the notion that only one set of chemically equivalent phosphine ligands is present in cation **[1Hy]$^+$**. The relatively large coupling constant of 22 Hz is characteristic of a *cis* relationship between the hydride and the phosphines, which thus have to reside in basal positions.[24]

The bridging hydride appears in the ^{1}H NMR spectrum of dication **[1HHy]$^{2+}$** as a doublet of doublets at $\delta =$ -15.6 ppm. The two $J_{H,P}$ coupling constants of 21 and 23 Hz are indicative of a coupling to two different phosphine nuclei and are in the same range as that found in cation **[1Hy]$^+$**. The signals of the trimethylphosphine protons appear as two doublets at $\delta = 1.57$ and 1.63 ppm, similar to the situation found in cation **[1H]$^+$**. This splitting can be explained by a restricted inversion of the azaheterocycle.[26]

Analogous to the situation in cation **[1H]$^+$**, two different phosphorus nuclei are observed in the ^{31}P NMR spectrum of dication **[1HHy]$^{2+}$**. However, in contrast to the spectrum of **[1H]$^+$**, each signal experiences an additional splitting as each phosphorus center couples to the bridging hydride. Each phosphorus nucleus therefore appears as a doublet of doublets at $\delta = 25.3$ and 21.3 ppm. The larger $J_{P,H}$ coupling constants of 21 and 23 Hz, respectively, are equivalent to those found for the bridging hydride in the ^{1}H NMR spectrum and can thus be assigned to a coupling of each phosphorus center to the bridging hydride. In addition, two-dimensional ^{1}H-^{31}P correlation experiments show the coupling of each phosphorus nucleus to the hydride (see the Supporting Information). A small splitting of 5.2 Hz can be observed for both signals due to a coupling between the nonequivalent phosphorus centers, as found in the spectrum of cation **[1H]$^+$**.

It can be concluded from the information obtained by NMR spectroscopy that the two iron nuclei prefer a symmetric coordination of the trimethylphosphine ligands in solution in all protonation states. The density functional calculations also support this assignment as the NMR chemical shifts of all four states are in good agreement with the computational results (Table 1).

The electronic absorption spectra of **1** and its protonated forms (see Supporting Information) show that protonation of the Fe–Fe bond results in loss of the band at 354 nm ($\varepsilon =$

Table 1. Experimental and calculated ^{1}H and ^{31}P NMR spectra.

Complex	^{31}P NMR chemical shifts [ppm]		^{1}H NMR chemical shifts [ppm]	
	exptl[a]	calcd[b]	exptl[a]	calcd[b]
1(basal/basal)	23.2	25.2	1.50[c]	1.32[c]
[1H]$^+$	19.8, 31.1	21.5, 34.0	1.56,[c] 1.54[c]	1.39,[c] 1.50[c]
[1Hy]$^+$	21.9	21.9	−15.6[d], 1.53[c]	−10.8[d], 1.42[c]
[1HHy]$^{2+}$	21.3, 25.3	26.9, 29.7	−15.6,[d] 1.57[c], 1.63[c]	−10.8,[d] 1.40[c], 1.46[c]

[a] In [D_3]acetonitrile solution at 25 °C. [b] Relative to TMS. [c] ^{1}H NMR shifts of the trimethylphosphine protons averaged over all nine protons. [d] ^{1}H NMR shifts of the hydride.

9000 $M^{-1}cm^{-1}$), while N-protonation is associated with minor and less specific absorption changes. In view of kinetic measurements of the protonation reactions, the protonation state of the complex is therefore probed more sensitively by IR spectroscopy. In this context the CO ligands are useful spectator ligands as the carbonyl frequencies are sensitive to the electron density at the iron centers, which determines the extent of backbonding to the CO ligands. Protonation of the Fe–Fe bond results in a drastic increase of ν_{CO} by about 80 cm^{-1} due to a substantial decrease in the electron density, as formally expressed by the Fe^{II}-Fe^{II} valence state of the hydride complex.[27,28] Substantially smaller shifts of about 15 cm^{-1} are indicative of protonation of the adt ligand.[21,29,30] Our previous assignments[22] of the IR spectra (see Supporting Information) based on these arguments were confirmed by comparison with the calculated IR spectra (Table 2), as the spectral shifts predicted for the different protonation states are in good agreement with the experimental data.

Table 2. Experimental and calculated IR data.

Complex	Exptl $\tilde{\nu}_{max}$ [cm^{-1}] (ε [$M^{-1}cm^{-1}$])	Calcd $\tilde{\nu}_{max}$ [cm^{-1}]
1	1981 (1860), 1943 (3530), 1908 (2060), ≈1890 (sh)	1963, 1946, 1915, 1901
[1H]$^+$	1999 (790), 1962 (3360), 1922 (2000) ≈1910 (sh)	1991, 1961, 1947, 1917
[1Hy]$^+$	2033 (3660), 1992 (2460)	2031, 2023, 1987, 1985
[1HHy]$^{2+}$	2048 (3670), 2008 (2150)	2051, 2043, 2006, 1991

[a] In acetonitrile solution at 25 °C.

Protonation reactions: The different protonation states of **1** can be interconverted by the reactions indicated in Scheme 2. The formation of two monoprotonated states of the dibasic complex was an intriguing finding and we therefore set out to investigate the protonation reactions in more detail. The reactions were monitored by IR spectroscopy by following the strong absorptions in the carbonyl range that provide characteristic signatures for all protonation states. All reactions were investigated in acetonitrile solution and all pK_a values refer to this solvent.

Protonation of the adt nitrogen: Initial protonation of **1** with stoichiometric amounts of strong acids such as triflic acid (HOTf, pK_a = 2.60)[31] or perchloric acid (pK_a = 2.0)[31] occurs at the adt nitrogen to give cation **[1H]$^+$** quantitatively, whereas **1** is only partly protonated by the weaker trifluoroacetic acid (pK_a = 12.65).[31] The pK_a of **[1H]$^+$** (p$K_{a(1)}$ = 12) was determined from the equilibrium concentrations of **1** and **[1H]$^+$**. Titrations with sub-stoichiometric amounts of perchloric and triflic acid showed several well preserved isosbestic points, thus proving that the protonation product is formed in a uniform reaction. Complex **1** can be quantitatively recovered by deprotonation with, for example, triethanolamine (pK_a = 15.93),[31] which proves the chemical integrity of cation **[1H]$^+$**.

Protonation of the Fe–Fe bond: In contrast to perchloric acid (see above), reaction of **1** with hydrochloric acid (pK_a ≈8)[31,32] results ultimately in the metal-protonated complex **[1Hy]$^+$**. Time-resolved IR spectroscopy revealed, however, that the initial protonation product is again the N-protonated complex **[1H]$^+$**. The spectra in Figure 2 show how the transiently formed cation **[1H]$^+$** undergoes tautomerization to the metal-protonated complex, which indicates that the Fe–Fe bond is more basic than the adt nitrogen of **1**. This is also supported by the results of density functional calculations, which predict a stabilization of **[1Hy]$^+$** by 17.6 kJ mol^{-1} (33.5 kJ mol^{-1} in vacuo) relative to **[1H]$^+$**. The value of $\Delta G^{o}_{(5)}$ (−17.6 kJ mol^{-1}) indicates that the tautomerization equilibrium should be completely on the side of the hydride **[1Hy]$^+$** (p$K_{(5)}$ = −3.1 at 298 K). Based on this value we can estimate the pK_a value of **[1Hy]$^+$** (p$K_{a(4)}$) as being 15 from the thermodynamic cycle (reactions 1, 5, and 4 in Scheme 2).

The tautomerization kinetics are first-order in hydrochloric acid, with a bimolecular rate constant, $k_{(5,HCl)}$, of 2.2 $M^{-1}s^{-1}$. The intercept of the extrapolated pseudo-first-order plot would indicate a tautomerization time of 100 s in the absence of HCl. However, no spontaneous tautomerization can be observed, even over much longer time-scales, when the metastable cation **[1H]$^+$** is generated with, for example, perchloric or trifluoroacetic acid. The HCl-catalyzed tautomerization can also be observed when sub-stoichiometric amounts of HCl are added to a solution containing **[1H]$^+$** generated by addition of perchloric acid, which results in slow transformation into the cation **[1Hy]$^+$**. The reaction is also first order in HCl under these conditions and proceeds with a similar bimolecular rate constant. The observed rate for the formation of cation **[1Hy]$^+$** is unaffected when equilibrium 1 (Scheme 2) is forced to the left by addition of tetrabutylammonium perchlorate to a solution of **[1H]$^+$** formed by addition of perchloric acid. It can therefore be excluded that the HCl-catalyzed tautomerization proceeds by reaction of HCl with unprotonated **1** (Scheme 2, reac-

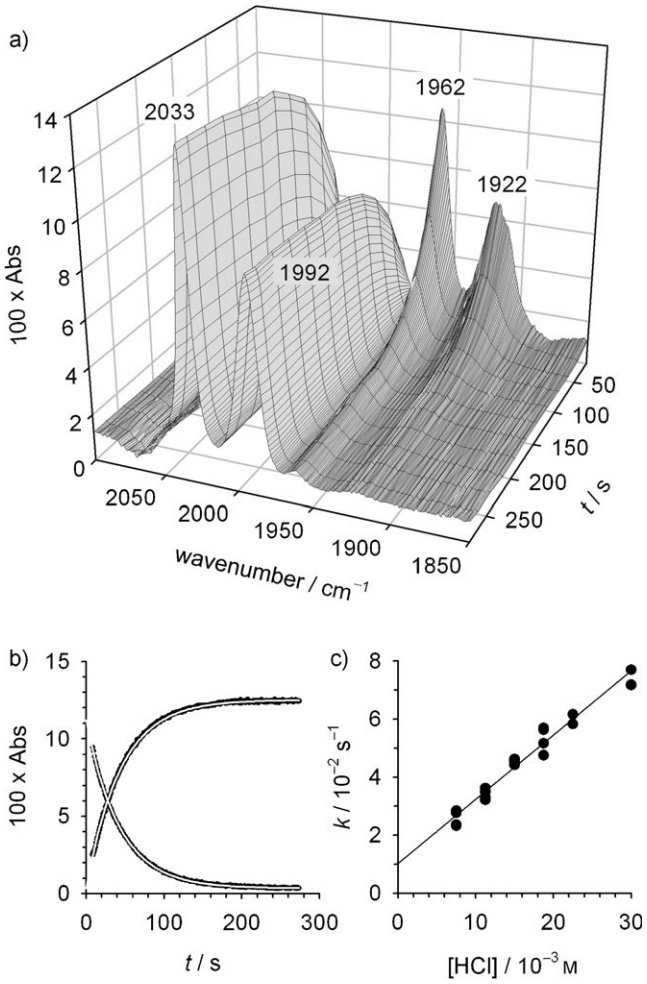

Figure 2. Protonation of **1** (0.3 mM) with HCl in acetonitrile solution (optical path length $l=1$ mm). a) Time-resolved IR spectra after reaction of **1** with HCl (7.5 mM). b) Kinetic traces and exponential fits for the decay of $[\mathbf{1H}]^+$ (1962 cm^{-1}) and the formation of $[\mathbf{1Hy}]^+$ (2033 cm^{-1}); [HCl]= 7.5 mM. c) A plot of the pseudo-first-order rate constants vs. concentration of HCl gives a linear fit with a slope of $k_{(5,HCl)}=2.2\ M^{-1}s^{-1}$.

tion 4) in a pre-equilibrium mechanism. Given the pK_a values of the two protonation sites ($pK_{a(2)}=8$, $pK_{a(3)}=5$, see below) relative to HCl, protonation of cation $[\mathbf{1H}]^+$ at the Fe–Fe bond by HCl and subsequent *or* concerted deprotonation of the adt nitrogen by Cl^- are conceivable mechanisms for the tautomerization. In the case of a sequential mechanism it can be assumed that hydride formation (Scheme 2, reaction 2) is the rate-limiting step rather than the protolytic equilibrium at the adt nitrogen. Both mechanisms are therefore in agreement with the fact that dication $[\mathbf{1HHy}]^{2+}$ is not observed as an intermediate in the $[\mathbf{1H}]^+ \rightarrow [\mathbf{1Hy}]^+$ tautomerization.

Protonation of the adt nitrogen in cation ***[1Hy]***$^+$: Further protonation of $[\mathbf{1Hy}]^+$ to form dication $[\mathbf{1HHy}]^{2+}$ does not occur even with a large (200-fold) excess of HCl (0.6 M). This indicates that protonation of the Fe–Fe bond renders the adt nitrogen significantly less basic. Protonation of $[\mathbf{1Hy}]^+$ to $[\mathbf{1HHy}]^{2+}$, in fact, requires perchloric or triflic acid and a $pK_{a(3)}$ value of 5 was determined from the equilibrium concentrations after deprotonation with 2-nitroaniline ($pK_a=4.8$).[31]

If an excess of perchloric or triflic acid is used to generate cation $[\mathbf{1H}]^+$, subsequent reaction with HCl results in the formation of dication $[\mathbf{1HHy}]^{2+}$ with a rate constant similar to that of the tautomerization reaction. Similarly, $[\mathbf{1HHy}]^{2+}$ is formed by reaction of **1** with a mixture of HCl and $HClO_4$, where the instantaneously formed cation $[\mathbf{1H}]^+$ transforms slowly into dication $[\mathbf{1HHy}]^{2+}$. In both cases $[\mathbf{1Hy}]^+$ is not observed as an intermediate and it can be concluded that the $[\mathbf{1H}]^+ \rightarrow [\mathbf{1Hy}]^+$ tautomerization is the initial and rate-limiting step and is followed by rapid protonation of the adt nitrogen.

Protonation of the Fe–Fe bond in cation ***[1H]***$^+$: Reaction of **1** with an excess of triflic acid results in the instantaneous formation of cation $[\mathbf{1H}]^+$, which slowly evolves into dication $[\mathbf{1HHy}]^{2+}$ in the space of a few minutes. The rate of hydride formation is first order in acid and a bimolecular rate constant, $k_{(2,HOTf)}$, of 0.15 $M^{-1}s^{-1}$ was obtained from exponential fits of the IR absorption changes under pseudo-first-order conditions (Figure 3).[33] Formation of dication $[\mathbf{1HHy}]^{2+}$ is even slower with perchloric acid, and cation $[\mathbf{1H}]^+$ is the only detectable protonation product for several minutes with an $HClO_4$ concentration of less than 20 mM. No transformation of the initially formed cation $[\mathbf{1H}]^+$ into dication $[\mathbf{1HHy}]^{2+}$ could be observed over several hours in the presence of trifluoroacetic acid, even at high acid concentrations (130 mM), thus indicating that the Fe–Fe bond is substantially less basic in $[\mathbf{1H}]^+$ ($pK_{a(2)}<12$) than in **1**. A $pK_{a(2)}$ value of 8 can be estimated for the hydridic proton in dication $[\mathbf{1HHy}]^{2+}$ from the thermodynamic cycle (reactions 5, 3, and 2 in Scheme 2) with a $pK_{(5)}$ value of -3 and a $pK_{a(3)}$ value of 5.

Hydrobromic acid ($pK_a=5.5$)[31] forms dication $[\mathbf{1HHy}]^{2+}$ in a rapid reaction with no detectable intermediate and a lower limit of the bimolecular rate constant, $k_{(2,HBr)}$, of more than $10^2\ M^{-1}s^{-1}$ can be estimated. This implies that the rate-limiting hydride formation step is three orders of magnitude faster with HBr than with triflic acid if it is assumed that dication $[\mathbf{1HHy}]^{2+}$ is formed by the same reaction sequence (reactions 1 and 2 in Scheme 2). Deprotonation of this dication with triethanolamine occurs at the adt nitrogen[21,29,30] (reaction 3 in Scheme 2) while the hydridic proton of cation $[\mathbf{1Hy}]^+$ is inert towards the nitrogen base and **1** could only be recovered by deprotonation of this cation with tetrabutylammonium chloride (reaction 4 in Scheme 2).

Scheme 3 summarizes the characteristics of the protolytic equilibria. As the Fe–Fe bond is the more basic site, initial protonation of the adt nitrogen must be attributed to a kinetic effect, that is, slow hydride formation. The protonation/deprotonation kinetics for transition metal hydrides are generally slower than the rapid protolytic equilibria of oxygen and nitrogen acids and bases, and this behavior is usually attributed to the higher activation barrier arising

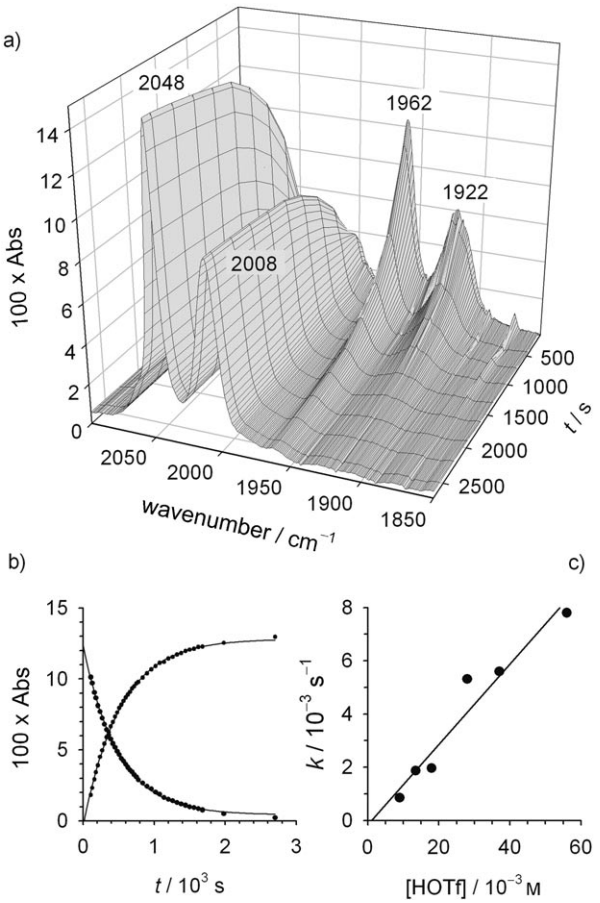

Figure 3. Protonation of **1** (3 mM) with triflic acid (HOTf) in acetonitrile solution (optical path length $l = 125\ \mu m$). a) Time-resolved IR spectra after reaction of **1** with HOTf (18 mM). b) Kinetic traces and exponential fits for the decay of $\mathbf{[1H]^+}$ ($1962\ cm^{-1}$) and the formation of $\mathbf{[1HHy]^{2+}}$ ($2048\ cm^{-1}$); [HCl] = 18 mM. c) A plot of the pseudo-first-order rate constants versus concentration of HOTf gives a linear fit with a slope of $k_{(2,HOTf)} = 0.15\ M^{-1}s^{-1}$.

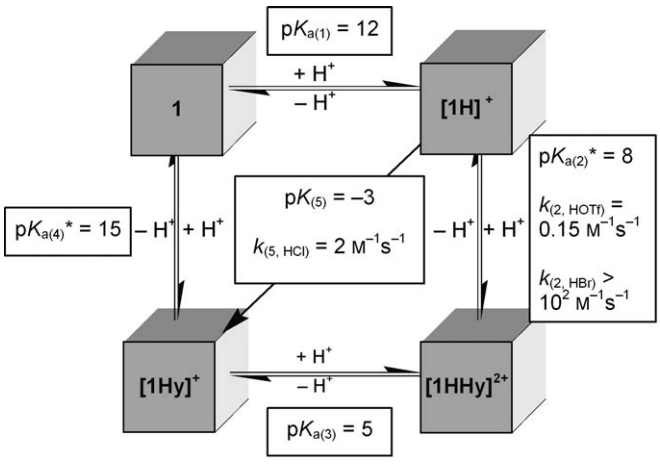

Scheme 3. Thermodynamic and kinetic characteristics of the protolytic equilibria connecting the four protonation states of **1** in acetonitrile solution. Rate constants describe the *protonation* reactions and equilibrium constants are given for the *de*protonations. Data marked with (*) were calculated on the basis of thermodynamic cycles and involve $pK_{(5)}$, which was derived from computational results.

from electronic and structural rearrangements typically associated with the formation/cleavage of a metal–hydride bond.[34] In addition, the Fe–Fe bond of **1** is particularly crowded due to the bulky phosphine ligands, which means that steric hindrance might contribute to the exceptionally slow kinetics of hydride formation by acids other than the smaller hydrohalic acids. Alternatively, the halides could promote oxidative addition of the proton to the iron centers if the nucleophilic counterion is transiently coordinated to the metal, which would stabilize the transition state.[35]

Electrochemical reduction: The electrochemical properties of **1** and its protonated forms were investigated to determine the effect of protonation on the reduction potentials. The protonated states were generated in situ under conditions established by the spectroscopic measurements; the electrochemical data are compiled in Table 3. Figure 4a shows differential pulse voltammograms (DPVs) of the complexes in acetonitrile solution. Compared to the hexacarbonyl analogue,[21] the electron-donating effect of the phosphine ligands shifts the reduction peak of **1** by 0.65 V towards a more cathodic potential. In analogy to similar diiron complexes, this peak can be assigned to a metal-centered reduction that results initially in the Fe^0Fe^I state. The irreversibility of the corresponding cyclic voltammogram (not shown) indicates that the primary reduction product is unstable on the voltammetric timescale, which has been attributed to ligand exchange and dimerization in the case of the related hexacarbonyl complexes.[19,36]

Table 3. Electrochemical data in acetonitrile solution.

Complex	$E^{[a]}$ [V] versus $Fc^{+/0}$	
	first oxidation	first reduction
1	−0.26	−2.18
$\mathbf{[1H]^+}$	0.01	−1.55[b]
$\mathbf{[1Hy]^+}$	0.65	−1.10
$\mathbf{[1HHy]^{2+}}$	1.38	−1.00

[a] DPV peak potentials. [b] Peak potential dependent on acid concentration.

The positive charge on the protonated adt nitrogen in cation $\mathbf{[1H]^+}$ fully compensates for the electronic effect of the phosphine ligands and the reduction peak is shifted towards more positive potential by around 0.7 V relative to the unprotonated complex. An even more pronounced shift of more than 1 V relative to the unprotonated complex is observed with the hydride complex $\mathbf{[1Hy]^+}$. This effect can be attributed to the significantly reduced electron density at the iron centers, as formally expressed by the Fe^{II}–Fe^{II} oxidation state of the hydride species. The least negative potential (−1.0 V) is found for the reduction of the doubly protonated complex $\mathbf{[1HHy]^{2+}}$, although the additional shift introduced by the second protonation amounts to only 0.5 V relative to the N-protonated complex $\mathbf{[1H]^+}$ and 0.1 V relative to the hydride $\mathbf{[1Hy]^+}$.

The magnitude of the reduction peak at around −1.5 V for cation $\mathbf{[1H]^+}$ increases with the concentration of

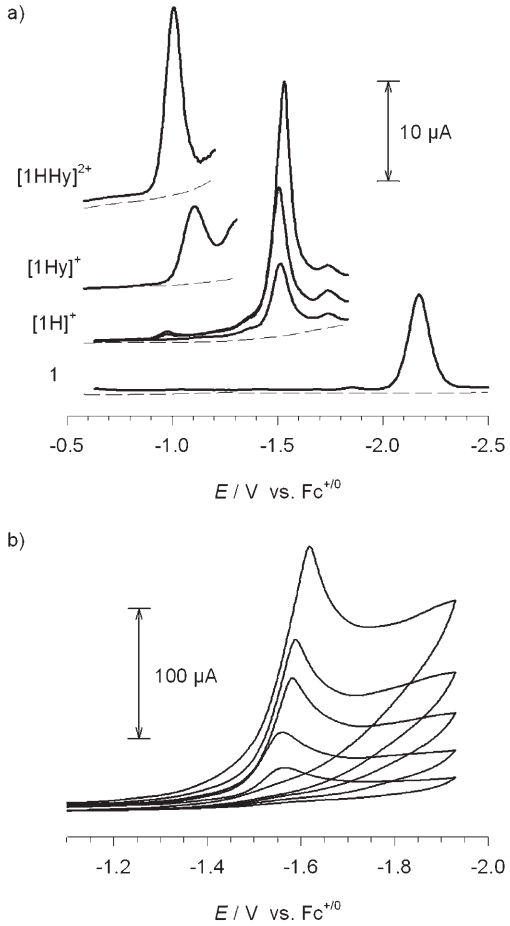

Figure 4. a) Differential pulse voltammograms (cathodic current up) on a glassy carbon electrode in acetonitrile solution. **1**: **1** (1 mM) without acid. **[1H]$^+$**: **1** (1 mM) with $HClO_4$ (3, 6, and 9 mM). **[1Hy]$^+$**: **1** (1 mM) with HCl (25 mM). **[1HHy]$^{2+}$**: **1** (1 mM) with $HClO_4$ (29 mM) and HCl (25 mM). Background scans for the indicated acid concentrations (9 mM $HClO_4$ for **[1H]$^+$**) are indicated by a dashed line. b) Cyclic voltammograms (0.1 V s^{-1}) of **[1H]$^+$** on a glassy carbon electrode in acetonitrile solution: **1** (1 mM) with $HClO_4$ (10, 20, 35, 60, 90 mM).

perchloric acid. This increased current can be attributed to catalytic proton reduction triggered by the reduction of **[1H]$^+$**, and the peak-shaped cyclic voltammograms and linearly increasing peak currents (Figure 4b) can be rationalized in terms of a completely catalytic situation where diffusion of the substrate controls the current (total catalysis).[37,38] The catalytic formation of H_2 certainly involves the reaction between a proton and a hydride intermediate[39] and the rapid turnover indicates that hydride formation is no longer kinetically constrained after reduction of the complex. The lower barrier for hydride formation after reduction could be due to an increased electron density or even associated structural changes of the ligand sphere. No increase of the voltammetric peak at −1.1 V was observed for cation **[1Hy]$^+$**, thereby indicating that reduction of the hydride complex does not result in catalytic turnover on the voltammetry timescale. The reduction peak at −1.0 V for dication **[1HHy]$^{2+}$** is higher than the diffusion-limited peak of **1**, although no further increase could be observed with triflic acid concentration (10–225 mM) even at sweep rates as low as 2 mV s^{-1}.[40] The absence of rapid catalytic turnover upon reduction of the doubly protonated complex could be due to its slow formation in the presence of triflic acid. However, no increase of the voltammetric current was observed even when hydrobromic acid was used to generate the dication. From the IR data it is evident that hydride formation with HBr is fast on the voltammetric timescale and it must therefore be concluded that turnover is limited by another step in the catalytic cycle.[41]

Only on the much longer time scale of bulk electrolysis (Figure 5) was slow catalytic proton reduction detected

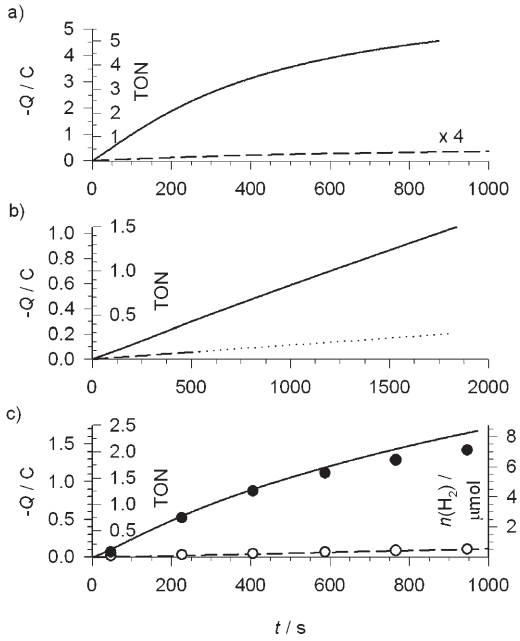

Figure 5. Controlled potential coulometry on a glassy carbon electrode in acetonitrile solution. Charge, Q, passed through the cell and turnover number (TON) with (——) and without the catalyst (-----). a) **[1H]$^+$**: **1** (1.6 mM) with $HClO_4$ (23 mM), 4.5 mL, −1.73 V. b) **[1Hy]$^+$**: **1** (1 mM) with HCl (120 mM), 3.5 mL, −1.18 V. c) **[1HHy]$^{2+}$**: **1** (1 mM) with $HClO_4$ (29 mM) and HCl (25 mM), 3.5 mL, −1.13 V; the amount of H_2 detected with (●) and without (○) catalyst is shown.

when cation **[1Hy]$^+$** and dication **[1HHy]$^{2+}$** were reduced at potentials close to their reduction peaks of −1.1 and −1.0 V, respectively. The formation of hydrogen with a faradaic yield of close to unity was confirmed by gas chromatography, although IR spectroscopic analysis of the electrolyzed solutions also revealed significant degradation of the catalyst after a few turnovers. It cannot therefore be excluded that at least part of the catalytic effect might arise from degradation products, including the possibility of heterogeneous catalysis by insoluble products.

A comparison of the catalytic reactions starting from the different protonation states in terms of overpotentials must consider the pK_a of the acids required to generate these protonation states.[42] The standard potential for the reversible reduction of protons from an acid, HA, is given by $E^{o}_{(HA)}=$

$E^{o}_{(H^+)} - (2.3\,RT/F)\,pK_{a(HA)}$, and under typical voltammetric conditions the half-wave potential is a good approximation of $E^{o}_{(HA)}$.[43] Taking into account an $E^{o}_{(H^+)}$ value of -0.14 V[42] for acetonitrile solution, the standard potentials of the acids employed in this study are $E^{o}_{(HClO_4)} = -0.26$, $E^{o}_{(HOTf)} = -0.29$, $E^{o}_{(HBr)} = -0.46$, and $E^{o}_{(HCl)} = -0.61$ V. This results in approximate overpotentials of 1.3 (**1H**$^+$, $HClO_4$), 0.5 (**1Hy**$^+$, HCl), 0.7 (**1HHy**$^{2+}$, HOTf), and 0.5 V (**1HHy**$^{2+}$, HBr).

Conclusion

Complex **1** forms two singly protonated states, namely the metal-protonated cation **[1Hy]**$^+$ and the ligand-protonated cation **[1H]**$^+$, as well as the doubly protonated cation **[1HHy]**$^{2+}$, which contains a proton and a hydride simultaneously. These four protonation states can be prepared selectively and have been characterized by spectroscopy. The solution structure of all protonation states is characterized by a basal/basal orientation of the phosphine ligands that contrasts with the basal/apical solid-state structure of **1**.

The hydride **[1Hy]**$^+$ is the thermodynamically more stable of the two singly protonated complexes while formation of the metastable cation **[1H]**$^+$ is kinetically favored. Tautomerization of the latter occurs only in the presence of hydrochloric acid, which allows for the selective preparation of the two tautomers. Formation of the doubly protonated dication **[1HHy]**$^{2+}$ by hydride addition to **[1H]**$^+$ is an exceptionally slow reaction with triflic acid. Faster formation of this dication follows a different mechanism with hydrochloric acid as the tautomerization catalyst in combination with stronger acids that are capable of protonating the adt nitrogen of **[1Hy]**$^+$. The dicationic complex **[1HHy]**$^{2+}$ is generated most rapidly in the reaction with hydrobromic acid, which can follow either of two mechanisms. The main advantage of the smaller hydrohalic acids in hydride formation is either a result of their lower steric hindrance or the electronic properties of the nucleophilic halides, which could coordinate transiently to the iron centers during the course of the oxidative addition of the proton.

The doubly protonated complex **[1HHy]**$^{2+}$ is the most easily reduced not only among the four protonation states discussed here but all currently known iron hydrogenase active-site mimics. Structures capable of binding a proton and a hydride prior to reduction are therefore an attractive strategy for the development of future synthetic catalysts. Our results indicate, however, that the kinetic limitations for hydride formation can be severe at the Fe^I level, that is, without reduction preceding the oxidative addition of the proton to the metal center. Even though hydride formation is probably not the rate-limiting step in the catalytic turnover of the particular complex investigated in this study, it could easily become rate-limiting for the catalysis by related structures. Such limitations obviously do not hamper the rapid turnover of the enzyme, however, where hydride formation is certainly promoted by the availability of an open coordination site. For the design of prospective models this implies that a loosely bound, easily exchangeable ligand[44] is a promising feature which might possibly solve the problems encountered in this study.

Experimental Section

General procedures: *p*-Formaldehyde, benzylamine, thionyl chloride, and trimethylphosphine were purchased from commercial suppliers and were used as received. Tetrahydrofuran was distilled from sodium/benzophenone under nitrogen atmosphere. Dichloromethane was distilled from calcium hydride under a nitrogen atmosphere. Flash chromatography was performed on Merck silica gel SI-60 Å (35–70).

Protonation reactions were performed with perchloric acid (70–72% aqueous solution, Merck, analytical grade), triflouromethanesulfonic acid (Sigma-Aldrich, 99%), hydrochloric acid (37% aqueous solution, Fluka, Ph. Eur), non-aqueous hydrochloric acid (1.25 M in ethanol, Fluka, puriss. p.a.), trifluoroacetic acid (Merck, analytical grade), or hydrobromic acid (33 wt.% in acetic acid, Sigma-Aldrich). Triethanolamine (Merck, analytical grade), 2-nitroaniline (Fluka, $\geq$98%), and tetrabutylammonium chloride hydrate (Aldrich, 98%) were used for deprotonation. All sample preparations for spectroscopic characterization were carried out with strict exclusion of oxygen in an argon-filled glove-box where samples were transferred into NMR tubes equipped with gas-tight caps or to a gas-tight IR cell. Less rigorous exclusion of oxygen resulted in degradation reactions that prevented isolation of the protonated complexes.

$[Fe_2(\mu\text{-adt})(CO)_6]$ (2): This complex was synthesized from diironhexacarbonyl disulfide.[17] It was purified by flash chromatography on silica gel (pentane:toluene = 90:10) and obtained as a red solid (345 mg, 68%). Single crystals were grown from concentrated *n*-hexane solutions. ^{1}H NMR (400 MHz, $CDCl_3$, 25 °C, TMS): δ = 7.30–7.26 (m, 3H; Ar*H*), 7.17 (d, J = 6.5 Hz, 2H; Ar*H*), 3.71 (s, 2H; NCH_2Ph), 3.34 ppm (s, 4H; SCH_2N); ^{13}C NMR (100.6 MHz, $CDCl_3$, 25 °C, TMS): δ = 208.0, 136.1, 128.9, 128.8, 127.6, 62.2, 52.7 ppm; IR (*n*-hexane): $\tilde{\nu}$ = 2075, 2036, 2004, 1998 cm^{-1} (C=O); elemental analysis calcd (%) for $C_{15}H_{11}Fe_2NO_6S_2$: C 37.76, H 2.32, N 2.94; found: C 37.94, H 2.46, N 3.07.

$[Fe_2(\mu\text{-adt})(CO)_4(PMe_3)_2]$ (1): This complex was prepared according to a reported procedure.[22] ^{1}H NMR (400 MHz, $CDCl_3$, 25 °C, TMS): δ = 7.30–7.26 (m, 3H; Ar*H*), 7.18 (d, J = 6.8 Hz, 2H; Ar*H*), 3.55 (s, 2H; NCH_2Ph), 3.08 (s, 4H; SCH_2N), 1.50 ppm (d, J = 9.2 Hz, 18H; *PMe*$_3$); ^{13}C NMR(100.6 MHz, [D$_8$]THF, 25 °C, TMS): δ = 217.5, 217.3, 137.9, 130.3, 129.1, 128.3, 63.8, 54.2, 20.8, 20.4 ppm (2C); ^{31}P NMR (161.9 MHz, CD_3CN, 25 °C): δ = 23.3 ppm; IR (acetonitrile): $\tilde{\nu}$ = 1980, 1943, 1907, 1892 cm^{-1} (sh) (C=O).

$[Fe_2(\mu\text{-Hadt})(CO)_4(PMe_3)_2]^+$ ([1H]$^+$): This complex was synthesized by addition of a small excess of $HClO_4$ to a solution of **1** in acetonitrile. ^{1}H NMR (400 MHz, CD_3CN, 25 °C, TMS): δ = 7.51–7.44 (m, 5H; Ar*H*), 4.32 (d, J = 5.2 Hz, 2H; NCH_2Ph), 3.95 (d, J = 12.4 Hz, 2H; SCH_aH_bN), 2.95 (dd, J = 11.2, 12.4 Hz, 2H; SCH_aH_bN), 1.56 (d, J = 10.4 Hz, 9H; *PMe*$_3$), 1.54 ppm (d, J = 9.6 Hz, 9H; *PMe*$_3$); ^{31}P NMR (161.9 MHz, CD_3CN, 25 °C): δ = 31.1 (d, J = 4.7 Hz), 19.8 ppm (broad); IR (acetonitrile): $\tilde{\nu}$ = 1999, 1991 (sh), 1961, 1921, 1912 cm^{-1} (sh) (C=O).

$[Fe_2(\mu\text{-H})(\mu\text{-adt})(CO)_4(PMe_3)_2]^+$ ([1Hy]$^+$): This complex was synthesized by addition of a small excess of HCl to a solution of **1** in acetonitrile. ^{1}H NMR (400 MHz, CD_3CN, 25 °C, TMS): δ = 7.52–7.27 (m, 5H; Ar*H*), 3.87 (m, 2H; NCH_2Ph), 3.53 (m, 4H; SCH_2N), 1.53 (d, J = 10.8 Hz, 18H; *PMe*$_3$), −15.61 ppm (dd, J = 22.0, 22.0 Hz, 1H; Fe*H*Fe); ^{31}P NMR (161.9 MHz, CD_3CN, 25 °C): δ = 21.9 ppm (d, J = 22 Hz); IR (acetonitrile): $\tilde{\nu}$ = 2033, 1991 cm^{-1} (C=O).

$[Fe_2(\mu\text{-H})(\mu\text{-Hadt})(CO)_4(PMe_3)_2]^{2+}$ ([1HHy]$^{2+}$): This complex was synthesized by addition of an excess of triflic acid to a solution of **1** in acetonitrile. ^{1}H NMR (400 MHz, CD_3CN, 25 °C, TMS): δ = 7.58–7.50 (m, 5H; Ar*H*), 5.72 (br., 1H; N*H*), 4.60 (d, J = 4.8 Hz, 2H; NCH_2Ph), 4.52–4.41 (m, 2H; SCH_aH_bN), 3.68 (m, 2H; SCH_aH_bN), 1.63 (d, J = 11.2 Hz, 9H; *PMe*$_3$), 1.57 (d, J = 10.8 Hz, 9H; *PMe*$_3$), −15.61 ppm (dd, J = 21.0,

23.0 Hz, 1H; Fe*H*Fe); ^{31}P NMR (161.9 MHz, CD_3CN, 25 °C): $\delta = 25.4$ (dd, $J = 23$, 5.2 Hz), 21.4 ppm (m); IR (acetonitrile): $\tilde{\nu} = 2048$, 2009 cm^{-1} (C=O).

NMR spectroscopy: ^{1}H NMR spectra were recorded with a Varian 400 MHz spectrometer for solution in CD_3CN or $CDCl_3$. Residual protic solvent peaks from $CHCl_3$ ($\delta_H = 7.26$ ppm) and CD_2HCN ($\delta_H = 1.95$ ppm) were used as internal references. ^{13}C NMR spectra were recorded with the same instrument operating at a frequency of 100.6 MHz using the central signals of $CDCl_3$ ($\delta = 77.0$ ppm) or [D_8]THF ($\delta = 67.57$ ppm) as reference signal. ^{31}P NMR spectra were recorded with a Varian 400 MHz instrument at 161.9 MHz, with chemical shifts referenced to external 85 % H_3PO_4 via the lock signal.

IR spectroscopy: IR absorption spectra were recorded between 1000 and 5000 cm^{-1} at a resolution of 1 cm^{-1} with a Bruker FT-IR spectrometer (IFS 66v/S) in a liquid-sample cell (Bruker A140) with CaF_2 windows and path-lengths of 125 μm or 1 mm. All solutions were prepared in acetonitrile (Merck, spectroscopic grade).

Electrochemistry: All electrochemical measurements were performed in an argon-filled glove-box. Cyclic voltammetry, differential pulse voltammetry, and controlled potential electrolysis were carried out with an Autolab potentiostat with a GPES electrochemical interface (Eco Chemie). The working electrode was a freshly polished, glassy carbon disc (diameter: 3 mm) for voltammetry. A glassy carbon rod in a compartment separated from the bulk solution by a fritted disk was used as counter electrode. The reference electrode was a non-aqueous Ag^+/Ag electrode (CH Instruments, 0.010 M $AgNO_3$ in acetonitrile) with a potential of −0.08 V versus the ferrocenium/ferrocene (Fc^+/Fc) couple in acetonitrile as an external standard. All potentials reported here are quoted relative to the Fc^+/Fc couple by adding −0.08 V to the potentials measured with the Ag^+/Ag electrode. All solutions were prepared with dry acetonitrile (Merck, spectroscopy grade, dried with 3-Å molecular sieves) with 0.1 M tetrabutylammonium hexafluorophosphate (Fluka, electrochemical grade) that had been dried in vacuo at 363 K as supporting electrolyte.

Gas chromatography: The concentration of hydrogen gas was monitored with a Varian CP4900 micro gas chromatograph (5-Å molecular sieve column, TLC detector) that was set to sample on-line from the headspace of the cathode chamber of the electrolysis cell. Calibration was made against H_2/Ar mixtures (Alphamix 3, AirLiquide). For the quantification of electrochemically produced H_2 the amount of dissolved H_2 could be neglected ($n_{sol}/n_{gas} = 0.0018$) since the liquid/head space volume ratio of the electrochemical cell was 0.019 and Henry's constant for H_2 in acetonitrile is 5.72 MPa at 298 K.[45]

Computational methods: All calculations were performed with the B-P86 functional,[46,47] which was selected for its known ability to reproduce the stereoelectronic features of transition metal complexes relevant to hydrogenases.[48]

A large triple-zeta basis set along with polarization functions (TZVP)[49] was employed for all atoms in the system. All the structures presented are minima on the DFT energy hypersurface, and all optimizations were carried out in vacuo and also independently in acetonitrile (COSMO). IR frequencies were obtained by analytical evaluation of the second derivative of the DFT energy expression. Thermodynamic corrections (approximated partition function) were used to evaluate the Gibbs free-energy difference between isomers. Furthermore, a conductor-like screening model (COSMO) was adopted to take into account solvation effects, using the dielectric constant of acetonitrile ($\varepsilon = 37$).[50]

Nuclear magnetic shielding tensors were computed using B-P86/TZVP geometries and the Gauge Including Atomic Orbital (GIAO) method.[51,52]

Acknowledgments

Adolf Gogoll is acknowledged for his assistance with the NMR measurements. Financial support for this work was provided by the Swedish Energy Agency, the Swedish Research Council, the Knut and Alice Wallenberg Foundation, and NEST, SOLAR-H (EU contract no. 516510). M.S. is grateful to the Klaus Tschira Foundation and the BMBF (grant no. 0313076) for financial support.

[1] N. S. Lewis, D. G. Nocera, *Proc. Natl. Acad. Sci. USA* **2006**, *103*, 15729–15735.
[2] M. Y. Darensbourg, E. J. Lyon, J. J. Smee, *Coord. Chem. Rev.* **2000**, *206–207*, 533–561.
[3] Y. Nicolet, C. Cavazza, J. C. Fontecilla-Camps, *J. Inorg. Biochem.* **2002**, *91*, 1–8.
[4] D. J. Evans, C. J. Pickett, *Chem. Soc. Rev.* **2003**, *32*, 268–275.
[5] M. W. W. Adams, E. I. Stiefel, *Curr. Opin. Chem. Biol.* **2000**, *4*, 214–220.
[6] I. P. Georgakaki, L. M. Thomson, E. J. Lyon, M. B. Hall, M. Y. Darensbourg, *Coord. Chem. Rev.* **2003**, *238–239*, 255–266.
[7] T. B. Rauchfuss, *Inorg. Chem.* **2004**, *43*, 14–26.
[8] L.-C. Song, *Acc. Chem. Res.* **2005**, *38*, 21–28.
[9] In particular, we have recently become interested in the potential application of hydrogenase mimics as molecular catalysts in light-driven hydrogen production, see: S. Ott, M. Kritikos, B. Åkermark, L. Sun, *Angew. Chem.* **2003**, *115*, 3407–3410; *Angew. Chem. Int. Ed.* **2003**, *42*, 3285–3288; S. Ott, M. Borgström, M. Kritikos, R. Lomoth, J. Bergquist, B. Åkermark, L. Hammarström, L. Sun, *Inorg. Chem.* **2004**, *43*, 4683–4692.
[10] J. W. Peters, W. N. Lanzilotta, B. J. Lemon, L. C. Seefeldt, *Science* **1998**, *282*, 1853–1858.
[11] Y. Nicolet, A. L. de Lacey, X. Vernède, V. M. Fernandez, E. C. Hatchikian, J. C. Fontecilla-Camps, *J. Am. Chem. Soc.* **2001**, *123*, 1596–1601.
[12] H.-J. Fan, M. B. Hall, *J. Am. Chem. Soc.* **2001**, *123*, 3828–3829.
[13] Y. Nicolet, C. Piras, P. Legrand, C. E. Hatchikian, J. C. Fontecilla-Camps, *Structure* **1999**, *7*, 13–23.
[14] Z.-P. Liu, P. Hu, *J. Am. Chem. Soc.* **2002**, *124*, 5175–5182.
[15] Z.-P. Liu, P. Hu, *J. Chem. Phys.* **2002**, *117*, 8177–8180.
[16] F. Gloaguen, J. D. Lawrence, T. B. Rauchfuss, *J. Am. Chem. Soc.* **2001**, *123*, 9476–9477.
[17] F. Gloaguen, J. D. Lawrence, T. B. Rauchfuss, M. Bénard, M.-M. Rohmer, *Inorg. Chem.* **2002**, *41*, 6573–6582.
[18] D. Chong, I. P. Georgakaki, R. Mejia-Rodriguez, J. Sanabria-Chinchilla, M. P. Soriaga, M. Y. Darensbourg, *Dalton Trans.* **2003**, 4158–4163.
[19] S. J. Borg, T. Behrsing, S. P. Best, M. Razavet, X. Liu, C. J. Pickett, *J. Am. Chem. Soc.* **2004**, *126*, 16988–16999.
[20] J.-F. Capon, F. Gloaguen, P. Schollhammer, J. Talarmin, *J. Electroanal. Chem.* **2004**, *566*, 241–247.
[21] S. Ott, M. Kritikos, B. Åkermark, L. Sun, R. Lomoth, *Angew. Chem.* **2004**, *116*, 1024–1027; *Angew. Chem. Int. Ed.* **2004**, *43*, 1006–1009.
[22] L. Schwartz, G. Eilers, L. Eriksson, A. Gogoll, R. Lomoth, S. Ott, *Chem. Commun.* **2006**, 520–522.
[23] Decoupling of the phosphorus nuclei results in a singlet instead of the doublet.
[24] X. Zhao, I. P. Georgakaki, M. L. Miller, R. Mejia-Rodriguez, C.-Y. Chiang, M. Y. Darensbourg, *Inorg. Chem.* **2002**, *41*, 3917–3928.
[25] In analogy to the ^{1}H NMR spectrum, further signals of considerably smaller amplitude are found at higher frequency for the geometrical isomer.
[26] As a result of the various dynamic restrictions, the aliphatic region is rather convoluted and is difficult to interpret.
[27] F. Gloaguen, J. D. Lawrence, T. B. Rauchfuss, M. Benard, M.-M. Rohmer, *Inorg. Chem.* **2002**, *41*, 6573–6582.
[28] R. Mejia-Rodriguez, D. Chong, J. H. Reibenspies, M. P. Soriaga, M. Y. Darensbourg, *J. Am. Chem. Soc.* **2004**, *126*, 12004–12014.
[29] J. D. Lawrence, H. Li, T. B. Rauchfuss, M. Bénard, M.-M. Rohmer, *Angew. Chem.* **2001**, *113*, 1818–1821; *Angew. Chem. Int. Ed.* **2001**, *40*, 1768–1771.
[30] H. Li, T. Rauchfuss, *J. Am. Chem. Soc.* **2002**, *124*, 726–727.
[31] K. Izutsu, *Acid-Base Dissociation Constants in Dipolar Aprotic Solvents*, Blackwell, Oxford, **1990**.

[32] Identical results were obtained with HCl diluted in acetonitrile from either aqueous stock solution (12 M) or stock solution in ethanol (1.25 M).
[33] To rule out any catalytic effect from fluoride contamination the triflic acid was treated with calcium triflate with no detectable effect on the rate of hydride formation.
[34] See, for example: R. G. Pearson, *Chem. Rev.* **1985**, *85*, 41–49, and references therein.
[35] If Fe–H bond formation was the rate-limiting step in the extremely slow formation of the hydride, a kinetic isotope effect, k_H/k_D, of more than 2 would be expected based on a force constant of at least 50 N m^{-1} for the Fe–H bond. The kinetic data obtained with different batches of deuterated triflic acid were, however, too scattered to be conclusive.
[36] S. J. Borg, J. W. Tye, M. B. Hall, S. P. Best, *Inorg. Chem.* **2007**, *46*, 384–394.
[37] With the given bulk concentrations ($C°_{acid}/C°_{cat} = 10$) and scan rate (0.1 V s^{-1}) a turnover rate in the order of 10^2 s^{-1} can be estimated from Saveant's kinetic zone diagram.[38] This corresponds to a bimolecular rate constant of the order of 10^4 M^{-1} s^{-1} for a rate-limiting step that is first order in acid.
[38] J. M. Savéant, K. B. Su, *J. Electroanal. Chem.* **1984**, *171*, 341–349.
[39] Given the unfavorable relative positions of the proton on the adt ligand and the bridging hydride, it appears more likely that the hydride is attacked by a bulk proton in a bimolecular reaction rather than by the adt proton in an intramolecular reaction.
[40] As the time constant of the CV experiment is given by RT/nFv, an upper limit of the turnover rate of the order of 10^{-1} s^{-1} can be estimated from these results, which would correspond to a bimolecular rate constant, k_{cat}, of less than 1 M^{-1} s^{-1} for a rate-limiting step that is first order in acid.
[41] Subsequent, less well-defined reduction peaks are observed for both hydride complexes ($[\mathbf{1Hy}]^+$ and $[\mathbf{1HHy}]^{2+}$) around −1.6 V that increase with higher acid concentrations. This might indicate that rapid turnover can be triggered at more negative potentials, which generates the doubly reduced hydride complexes that should be more reactive towards protons.
[42] G. A. N. Felton, R. S. Glass, D. L. Lichtenberger, D. H. Evans, *Inorg. Chem.* **2006**, *45*, 9181–9184.
[43] Independent of bulk concentrations, the ratio [HA]/[A$^-$] is approximately unity at the electrode at the half-wave potential (or DPV peak potential). At the same time, the solvent at the electrode will be saturated with H_2 ($p = 1$ bar) even with millimolar concentrations of acid.
[44] L. Schwartz, J. Ekström, R. Lomoth, S. Ott, *Chem. Commun.* **2006**, 4206–4208.
[45] E. Brunner, *J. Chem. Eng. Data* **1985**, *30*, 269–273.
[46] A. D. Becke, *Phys. Rev. A* **1988**, *38*, 3098–3100.
[47] J. P. Perdew, *Phys. Rev. B J1 - PRB* **1986**, *33*, 8822–8824.
[48] M. Bruschi, G. Zampella, P. Fantucci, L. De Gioia, *Coord. Chem. Rev.* **2005**, *249*, 1620–1640.
[49] A. Schaefer, C. Huber, R. Ahlrichs, *J. Chem. Phys.* **1994**, *100*, 5829–5835.
[50] A. Klamt, G. Schüürmann, *J. Chem. Soc. Perkin Trans. 1* **1993**, 799–805.
[51] R. Ditchfield, *Mol. Phys.* **1974**, *27*, 789–807.
[52] K. Wolinski, J. F. Hinton, P. Pulay, *J. Am. Chem. Soc.* **1990**, *112*, 8251–8260.

Received: January 5, 2007
Published online: June 13, 2007

